Mammographic structure: data preparation and spatial statistics analysis

Arthur E. Burgess

Radiology Dept., Brigham & Women's Hospital,

Harvard Medical School, 75 Francis St., Boston, MA 02115

ABSTRACT

Detection of tumours in mammograms is limited by the very marked statistical variability of normal structure rather than image noise. This presentation reports investigation of the statistical properties of patient tissue structure in digitized x-ray projection mammograms, using a database of 105 normal pairs of craniocaudal images.The goal is to understand statistical properties of patient structure, and their effects on lesion detection, rather than the statistics of the images *per se*, so it was necessary to remove effects of the x-ray imaging and film digitizing procedures. Work is based on the log-exposure scale. Several algorithms were developed to estimate the breast image region corresponding to a constant thickness between the mammographic compression plates. Several analysis methods suggest that the tissue within that region, assuming second-order stationarity, is described by a power law spectrum of the form $P(f) = A/f^{\beta}$, where f is radial spatial frequency and β is about 3. There is no evidence of a flattening of the spectrum at low frequencies. Power law processes can have a variety statistical properties that seem surprising to an intuition gained using mildly random processes such as smoothed Gaussian or Poisson noise. Some of these will be mentioned. Since P(f) is approximately a 3rd order pole at zero frequency, spectral estimation is challenging.

Keywords: mammography, digitized mammograms, image segmentation, spectral analysis, power-law noise,second order statistics, sequential pixel variance analysis

1. INTRODUCTION

Over the last decade there has been a wide spread effort to develop computer-aided diagnosis (CAD) techniques for mammography. This work has clearly demonstrated the difficulty of detecting breast tumors. CAD mass detection experiments at 90% true-positive rates typically give about 2 false positives per image[1]. There have also been efforts to classify breast tissue [2,3,4,5,6]. This has been difficult because of the great variability of tissue structure. The purpose of the work described here is to obtain statistical results that can be used together with signal detection theory to predict lesion detection performance of various observer models as well as human observers.

The present work is based on a systematic approach designed to eliminate effects of the imaging system physics and geometry in order to allow statistical analysis of patient structure *per se*. Note that this approach is different from that of other papers in the literature which appear to base analysis directly on the digitized image data. One of the difficulties in dealing with this literature is the lack of methodological detail. For example, there are two main classes of digitizers, one gives output approximately proportional to light transmission and the other gives output approximately proportional to film optical density. Often, papers do not mention which type of digitizer scale is used. Since the scales are related by a logarithmic transformation, one would expect a marked difference in some statistical properties. For reasons discussed below, the work reported here will be based on a log-exposure amplitude scale. Only craniocaudal (CC) views were used in the present work because image segmentation is more straight-forward for this view.

The results presented below demonstrate that breast structure appears to have an approximately isotropic 2D power law spectrum of the form, $P(f)=K/f^{\beta}$, with β in the range from 2 to 4 (mean about 3), where f is radial frequency. This exponent range is identical to that of fractal surfaces. However, the term 'fractal' implies an number of other properties in addition spectrum slope so the generic term "power law process" will be used in this paper to encompass a large variety of possible processes.A number of authors have reported estimates of fractal dimension for selected regions of mammogram. Some

estimates have been based on spectral analysis of a small number of images[7,8]. Other authors have used indirect methods to estimate fractal dimension[9,10]. One must be concerned about the accuracy of such estimates because there are sources of severe systematic error with both spectral[11,12] and fractal-dimension based methods[13,14,15].

The term "fractal" in the context of mammograms is controversial. Many people assert that mammogram structure could not possibly be fractal while others seem quite happy to assume that the structure is fractal. These issues will be discussed in a subsequent paper[16]. Fractal processes can be deterministic or stochastic and have 2D radial spectra, $1/f^{\beta}$, with exponents between 2 and 4. Strictly speaking, the term "random fractal" applies to processes based on fractional Brownian motion that extend over an infinite range of scale [17].

There are many aspects to mammogram statistics and many possible approaches. Heine et al.[18] have used the multiresolution wavelet approach with separate analysis of each expansion component. The raw images were digitized from films with an amplitude scale approximately proportional to light transmission. They found that the component histograms could be modeled using families of Laplace probability density functions and reported a power-law spectrum $1/f^{\beta}$, with average exponent of 3. Rolland et al.[19] have used an approach based on higher order spatial statistics. The results presented here should be regarded as a preliminary exploration of second-order statistics of breast structure *per se*. It may eventually be possible to obtain an understanding of the underlying 3D processes that give rise to the observed breast structure statistics. However, this is a difficult inverse problem. For the moment, attention will be focused on assessing the reliability and consistency of existing techniques for statistical analysis, as well as adapting techniques from other fields and developing new analysis tools. There is a related presentation in the Image Perception conference[20] which will elaborate on the consequences of power law spectra for Monte Carlo simulation and lesion detection.

2. DATA PREPARATION

2.1. Image database

The digitized mammogram data were obtained from Dr. Larry Clarke of the Univ. of South Florida. There were a total of 105 normal cases with 4 images per case (left and right breast, craniocaudal and mediolateral oblique views). The film mammograms came from two Moffitt Cancer Center screening center sources with a GE Senograph DMR mammography unit (1993 model) and a Lorad Transpo 350 (1992 model) mammography unit. Both installations used Dupont Microvision screens and Kodak Min-R (one-sided) film, grids and a 0.3 mm focal spot. Complete quality assurance measurement records are available for both units. The cases selected for the database were all believed to be normal and were imaged between 1994 and 1996. The criterion for selecting the cases were: no artifacts, no microcalcification clusters, absence of visible disease (BIRADS category 1) and a follow up examination two years later that also was disease free. The films were digitized using a DBA model R3000[21] with 30 micron sampling (14 bits per pixel) and then reduced to 60 micron sampling for subsequent use.. The digitizer gray level output value is nearly proportional to the light transmission of the film and related to local film optical density, D(x,y), by an exponential relationship.

2.2 Data amplitude representation

It was necessary to select a particular amplitude scale for the image data. The problem is illustrated by considering the digital image production chain. The first representation is the 2D map of xray exposure E(x,y) at the input to the image receptor or alternatively its logarithm, logE(x,y). This is converted by the nonlinear response of film-screen combination into an analog optical density image or map, D(x,y). The digitizer converts this to gray level value map, V(x,y). The decision as to which is the best representation depends on motivation. Since this paper is concerned with projected patient structure, the best choice appears to be one based on spatial x-ray linear attenuation coefficient values as projected to the image plane. This leads naturally to the log-exposure representation. Using the simplifying assumption of a monoenergetic x-ray beam, the logarithm of x-ray exposure value at image location (x,y) is given by the product, $\log E(x,y) = \mu_z(x,y)t(x,y)$, of patient part thickness, t(x,y), and average linear attenuation variation, $\mu_z(x,y)$, along the x-ray projection ray path from the image position to the x-ray focus. Finally, if the constant thickness region of the mammogram can be reliability located, then logE(x,y) will be proportional to $\mu_z(x,y)$ This simple model ignores a number of complicating factors such anode heel effect, beam hardening, spatial varying secondary radiation, random variation in film sensitivity and processor chemical concentration. The amplitude transformations do have the effect of correcting the measured data values (to first order) for the major aspects of nonlinear film response as well the physics of the digitizer and x-ray imaging system. The digitized images were first converted to an optical density scale using the calibration curve of the digitizer and then converted to the log-exposure scale using calibration data

supplied by Sterling Diagnostic Imaging[22]. There is considerable variation of apparent film speed and less marked variation in the shape of the H&D curve over time because of changes in processing conditions. So a fixed transformation from optical density to log-exposure must be regarded as an approximation.

2.3. Constant thickness region segmentation

The first step was to attempt to determine the boundaries of the region where breast tissue thickness is approximately constant, as illustrated in figure 1. The major problem is that this had to be done without "ground truth". So validation was be accomplished by indirect methods. A variety of *ad hoc* segmentation methods were developed and the principal evaluation approach was to assess correlation of results for the left and right breasts of all patient cases in the database. This assumes symmetry of breast size and breast positioning during image production, Byng et al.[10] reported a correlation of 0.94 for left/right comparison of entire projected CC breast areas.

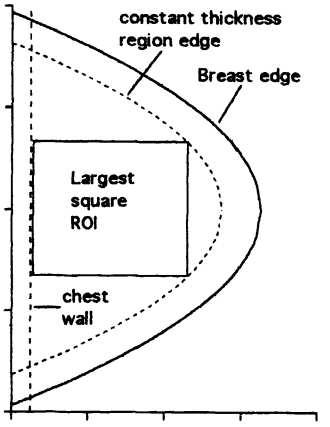

Figure 1. Outline of CC mammogram geometry. The outer boundary of the breast is approximately parabolic. The breast is between plastic compression plates, so there is a region of approximately constant thickness. Methods were developed to estimate the boundary of this region. The pectoral muscle (chest wall) is the proximal boundary of the breast tissue. The largest square ROI was estimated for analysis. The work presented here is based on 65 images with ROI size greater than or equal to 61 mm (1024 pixels, 60 micron sampling).

The images were reduced in size to 0.48 mm sampling for segmentation to reduce file size and computation time. The right craniocaudal images were flipped about the vertical axis so the chest wall was always on the left. This eliminated the left/right polarity difference and simplified computer coding. All programs and procedures were written in IDL[23]. The boundary of each breast was identified using an adaptive thresholding technique[24]. The threshold for each image was selected using the histogram of log-exposure values. The histograms contain sharp peaks for data values corresponding to the non-breast background region. It was found that the breast boundary could be fitted reasonably well by parabolic functions if the axes of the parabola coincided with the line half way between the upper and lower breast boundaries. The axes were not horizontal. This finding agrees with the report of Gooditt et al.[25] of the success of a second-degree polynomial fit. The apex of the parabola was used as an estimate of the distal boundary of the breast and eliminated protruding nipples from inclusion in subsequent segmentation steps.

The mammogram can be divided into two conceptual regions. A constant thickness region where the breast is in contact with the compression plates and a transition region of decreasing thickness as the breast boundary is approached. If breast tissue were homogeneous, the radiographic segmentation problem would be trivial. Unfortunately, parenchymal tissue is highly variable and extends into the transition region, so identification of the boundary of the (approximately) constant thickness region is difficult. Gooditt et. al.[25] report average values for the variation in film optical density in this transition region.

A preliminary evaluation of images using the IDL surface contour estimation procedure indicated that constant elevation curves in the transition region were approximately parallel to the breast boundary. This result suggested that an erosion procedure might be useful, if one could identify a stopping rule. Two approaches were attempted, based on the mean and standard deviation of the remaining image after each erosion step. This can referred to as an "onion-peeling" technique. The estimate of the constant thickness region size can be described as a fraction of the total projected breast area. It was found that the correlation between fraction for the left and right breasts cases was always less than about 0.65 for all stopping rules that were tried. So the "onion-peeling" method was abandoned. The second approach was based on a band parallel to the breast midline. The vertical extent of the band was arbitrarily selected to be 10% of the maximum vertical extent of each breast. The column pixel values within the band were averaged to yield a one-dimensional profile for subsequent analyses. Plots of band

data profiles are shown in figure 2. These examples were selected to illustrate the variety of profile shapes.

The starting point for analysis was the estimated distal point of the breast, based on the above parabolic boundary fit. The point of intersection, x_I, of the band with the constant thickness region was estimated by 3 methods. One used the smoothed derivative of the band data profile. The intersection point was taken to be the position of the zero crossing closest to the nipple. This approach gave a visually reasonable result for about 60% of the images. The second method of estimating the x_I intersection point was based on the mean data value for the band data over the range from the chest wall edge to 50% of the distance to the distal breast boundary. The second x_I value was taken to be the point where the decreasing band data profile first reached this mean value. The third method of estimating the intersection was by visual inspection of the band data profiles by the author. The final estimate of the x_I intersection was obtained as follows. If all these estimates were in good agreement, then the average value was used and the estimate was given a high confidence rating. If two values were in good agreement and the third was markedly different, then the average of the two agreeing values was used and the result was given a medium confidence rating. If all three values were very different, the subjective value was used and the result was give a low confidence rating. Chest wall muscle (pectoralis and sternalis) was apparent in some images and positions were identified by visual inspection. In all other images an arbitrary boundary was placed 7.7 mm from the chest wall edge of the mammogram.

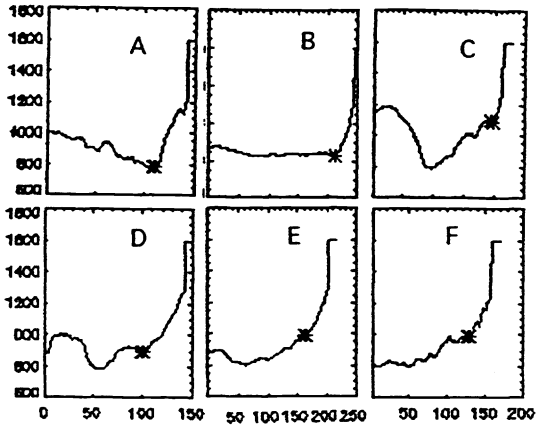

Figure 2. Representative band data examples.The * symbol indicates the estimated edge of the constant thickness region. Cases like A and B represented 60% of breasts.

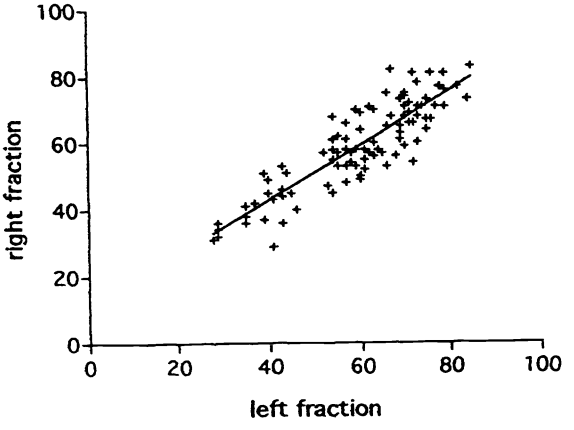

Figure 3. Correlation plot of constant thickness area fractions for of left and right breasts of each patient. The correlation is 0.88.

The value of x_I and the equation of the estimated breast midline were then used to identify a point (x_I, y_I) on the midline that was assumed to be on the boundary of the constant thickness region. Using the previous observation that contour lines were approximately parallel to the breast boundary, a binary version of the breast image was eroded (using a disc-shaped operator) until the (x_I, y_I) stopping point was reached. The boundary of the remainder was used as an estimate of the constant thickness region. This procedure was done for all 210 CC images in the database. There were a few cases where one of the breast fractions was very low while the other was not. In these cases the higher fraction was arbitrarily assigned to the breast with the low value. The correlation plot of left and right breast constant thickness area fractions of total breast area is shown in figure 3. The correlation of fractions was 0.88. This is slightly lower than the correlations of about 0.95 reported by Byng et al.[10] for comparisons of visual estimates of breast area and dense tissue fraction.

3. ROI MEANS AND VARIANCES

3.1. Over whole breast

In a preliminary step, the relationship between image data mean and variance was investigated. This was based on the optical density amplitude scale. Each breast was divided into 7.7 mm square regions of interest (ROIs) with 50% overlap. The mean

and standard deviation of the data in each square was then calculated. A scatter plot of standard deviation as a function of mean optical density (figure 4) demonstrates a strong dependence between these values due to the film H&D curve gradient (gamma) variation and tissue thickness variation. The value of gamma as a function of optical density, D, for the Microvision/Min-R system is described very well by a parabola, $\gamma(D) = 4.4 - 0.85(2.2-D)^2$. The scatter plot shows an similar trend for average and maximum standard deviation values. There was a peak in the vicinity of optical density equal to 2. Maps of standard deviation as a function of spatial position show a concentration of high values near the breast boundaries of each mammogram. In this region, the optical density tends to increase rapidly as breast thickness decreases. Tissue thickness gradients and gamma variation within the ROI lead to biased variance measurements and lead to a poor estimate of the spatial variation in tissue composition. These results support the view that statistical analysis of breast structure *per se* must be done within the constant thickness region and that log-exposure data values must be used.

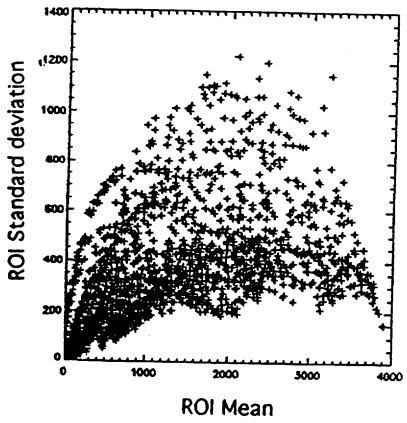

Figure 4. Scatter plot of ROI mean and standard deviation measurements for the whole breast with an optical density amplitude scale (zero on the scale corresponds to the base+ fog level). The correlation is due to film gamma and tissue thickness variation.

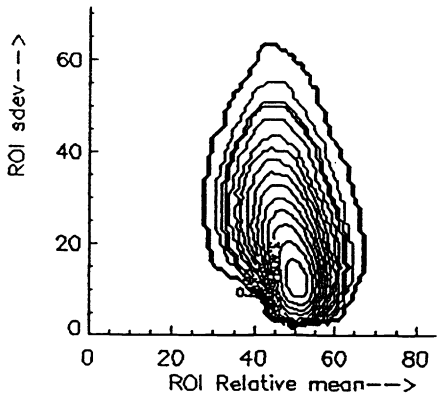

Figure 5. Contour plot of 2D histogram of ROI mean and standard deviation measurements for 210 CC images with constant thickness regions using the log-exposure scale (relative units). There is little correlation.

3.2. Within constant thickness region

The above analysis was repeated within the breast regions where thickness was estimated to be constant. The log-exposure amplitude scale was used. There were a total of 17,465 square non-overlapping regions for the 210 breasts. The paired measurements were placed in a 2D histogram to provide an estimate of the 2D probability density function, p(mean, std. dev.). The results are shown as a contour plot in figure 5. It is clear that, to a first approximation, there is very little correlation between ROI mean and ROI standard deviation. This result was surprising since it was expected that tissue complexity would be dependent on tissue physical density. This may be true for 3D breast tissue, but seems not to be true for projected data.

4. SPECTRAL DENSITY

4.1. Direct DFT method

Discrete Fourier transform (DFT) spectral analysis was done at two image resolutions (60 microns and 480 microns) within square regions. All images were evaluated to determine the size of the largest square bounded by the chest wall estimate and the edge of the constant thickness region. There were 65 images with squares larger than 6.1 cm (1024 pixels on a side, 60 microns sampling). These images were selected as a collection for spectral analysis using a 6.1 cm square data record centered on the largest possible square. Large records were used because, as will be seen below, there are problems associated with spectral analysis of small mammogram records. The word 'collection' is used rather than 'ensemble', because we do not yet know whether a single process model can account for all varieties of mammographic structure. No selection constraint other than the size was used, in order to eliminate further bias in sampling the population of breast patterns. The spectral analysis method[26] was direct in that the squared modulus of DFT of each 2D record was calculated to give a periodogram. The 65 periodograms were then averaged to give an estimate[11] of the 2D spectrum for the collection.

Two decisions must be made when doing DFT spectral analysis. One is the issue of mean subtraction, which influence the zero frequency (DC) value of the spectrum. The second is choice of a spatial data taper (also referred to as a window function). As will be seen below, these two issues are intimately related when spectra are sharply peaked at low frequency. The final result will be shown first and then the above issues will be discussed. Figure 6 is a shaded surface plot of the estimated 2D spectrum estimated for the collection, based on 0.48 mm sampling. It is sharply peaked at zero frequency and is approximately isotropic (little angular dependence). Note that the logarithm of spectral density was used. A surface plot with a linear spectral density scale would essentially look like a delta function. This is the source of analytical difficulty.

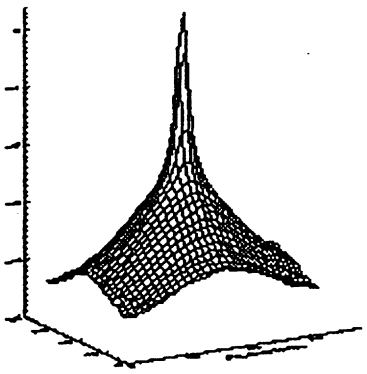

Figure 6. Shaded surface plot of the collection average power spectrum (log density scale) by direct DFT estimation. A radial Hanning data taper (window) was used. Note the lack of a strong angular dependence. A linear density scale plot would look like a delta function.

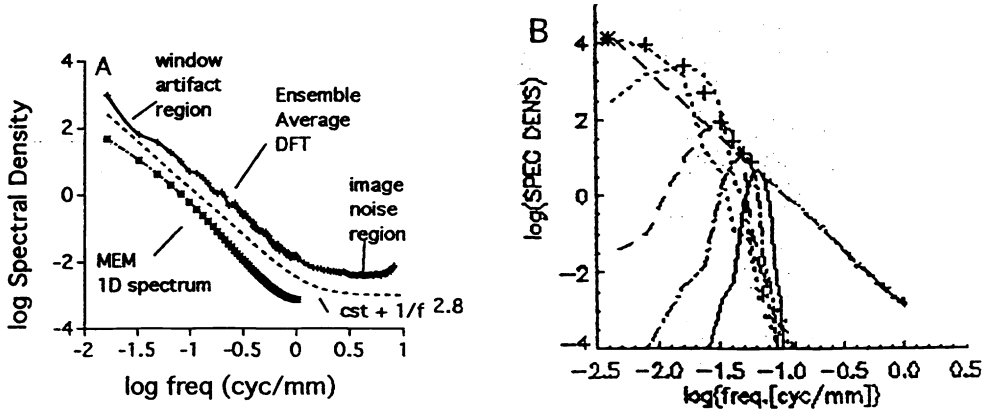

Figure 7. (A) Horizontal slice of the estimated average power spectrum (log-log scale) with relative density units. Both DFT and MEM results are shown. (B) The dotted curves represent the Fourier transform of the Hanning taper centered on selected frequencies to illustrate the effect of spectral leakage.

4.1.1. Data tapers

The DFT is periodic in that spatial data is implicitly repeated in both the x and y directions with period equal to the width of the square data record. The Fourier components of this periodic 2D function appear in the power spectrum (which is also periodic). If the 2D data record is used without modification, the implicit window is a 2D Rect function whose Fourier transform is readily apparent as a 2D sinc^2 function in the power spectrum of the mammogram collection. This effect is well known but not so readily apparent in less peaked spectra. The solution is to use a multiplicative data taper, t(x,y), so that if $d_k(x,y)$ is the k^{th} record, the product is $r_k(x,y)=d_k(x,y)t(x,y)$. The estimated power spectrum is given by the collection average result[11].

$$P(u,v) = \left\langle \left| D_k(u,v) ** T(u,v) \right|^2 \right\rangle_k \qquad (1)$$

based on the squared modulus of the 2D convolution of the Fourier transform of the image data, D(u,v), and the Fourier transform of the data taper, T(u,v), for spatial frequencies u and v. In the above equation, |...| denotes modulus, <...> denotes expectation value, and ** denotes 2D convolution. If no data taper is used, T(u,v) is replaced by the Fourier transform of the implicit 2D Rect window. The effect of convolution is to mix spectral values of nearby 2D frequency points - so-called "spectral leakage". This effect is particularly severe if the spectrum is sharply peaked at some frequency. Spectral leakage can be minimized but not eliminated by careful selection of a data taper. Various options are discussed in a number of publications[12]. Since the mammogram spectrum seemed to have little angular dependence, an isotropic taper function was used, based on a radial Hanning function adapted from the 1D version[11].

$$t(r) = 0.5(1 - \cos[\pi r/R]), \quad \text{for } r \le R \text{ and zero elsewhere} \qquad (2)$$

where R is the radius (in pixels) of the circular region and r is the taper radius measured from the center of the square mammogram record being analyzed.

4.1.2. Mean subtraction

The zero frequency value of the spectrum is equal to the variance of the mean values of individual records used in the collection. A decision must be made as to how the mean spatial value is to be defined. One option might be to subtract the mean value of each image from all data in that image. The effect of this operation would give a DC value of zero for the spectrum, which in turn would create a "hole" at the center of the spectrum. Convolution with the data taper would then artificially reduce all low-frequency spectral values. Similarly, a DC spectral value that is too high will artificially elevate all low-frequency values. The following approach was used for this work. The collection mean log-exposure value was determined the *complete* estimated constant thickness regions (not just the square record regions) of all 65 images in the collection. This estimated collection mean was then subtracted from the 6.1 cm square records used in spectral analysis.

4.1.3. 1D spectrum

The horizontal slice (f_y=0) of the collection average power spectrum is shown in figure 7A. It is a composite of analysis done using 60 micron sampling of 7.7 mm regions and 480 micron sampling of 6.1 cm regions. Correction has been made for the modulation transfer function of the min-R intensifying screen. Note that a double logarithmic scale has been used and that spectral density has been expressed in relative units. In figure 7B, the dotted curves associated with the low frequency data points represent the Fourier transform of the Hanning function data taper when shifted to those center frequencies. This gives an intuitive feel for the effect of the convolution described in equation (1). The point of this illustration is to show that there is marked systematic error in low frequency values because of spectra leakage from neighboring frequencies. One gets the subjective impression that the DFT spectral density values do not become reliable until a frequency of about 0.1 c/mm is reached. This is 6 times the sampling frequency (0.016 c/mm). In effect, most of the 6.1 cm square spatial record used for DFT analysis is wasted. If spectral leakage was not important, the same spectrum result could be attained using a square of about 1 cm on a side.

4.2. Parametric spectral analysis

There are other ways of estimating power spectra. The one chosen for this work is sometimes referred to as the maximum entropy method (MEM) or the Burg method[27]. It is based on the z-transform generalization of the DFT, using the relation $z = \exp(2\pi i f \Delta)$ where Δ is the 1D sampling distance. It is a 1D analysis method. So row and column projections of 2D data sets can be used to estimate 1D slices of the 2D spectrum, based on the projection-slice theorem (see Papoulis[28], who uses the term 'line spread function' for projection). Given a 1D sampled function $c_k=c(x_k)$ with locations x_k, the estimated power spectrum is

$$P_{MEM}(f) = \left| \sum_{k=-N/2}^{k=N/2-1} c_k z^k \right|^2 \approx \frac{a_0}{\left| 1 + \sum_{k=1}^{M} a_k z^k \right|^2} \qquad (3)$$

The equation version with c_k summation is a Laurent series approximation to the "true" power spectrum. This approximation can be replaced by another series approximation (involving a_k summation) with the free parameters in the denominator. The second approximation has a quite different character, since it can have poles on the unit circle of the z-domain (while corresponds to the real frequencies in the Nyquist interval). So it is a natural way of representing sharply peaked spectra. The summation limit, M, is the order of the approximation.

The main problem with this method is that an incorrect choice of M will lead to systematic error in the spectrum estimate. Several approaches were used in the present work. First, the DFT result suggested that the mammogram power spectrum was approximately, $P(f)=K/f^3$, which is a third order pole at zero frequency. Second, it is possible to simulate noise with the same spectrum by digital filtering and do MEM spectral analysis using a range of orders. It was found, as expectedly, that the best

MEM spectral estimated was obtained using a third order series (M = 3). MEM spectral estimates for each of the 6.1 cm square records were obtained using both row and column projections. This gave an estimate of the power law exponent of each record along both the f_x and f_y frequencies axes. A histogram of the exponents is shown in figure 8. The average MEM exponents were 3.0 (std. dev. 0.45) and 2.5 (std. dev. 0.3) in the f_y (vertical) and f_x (horizontal) directions respectively. The exponents covered the range from 1.8 to 3.8.

The advantage of the MEM method is that it should be, in principle, possible to do reliable spectral analysis of smaller spatial records. This is due to the fact that systematic error effects in MEM tend to be concentrated at high frequencies while DFT systematic error (due to spectral leakage) is concentrated at low frequencies. This avenue of investigation remains to be explored.

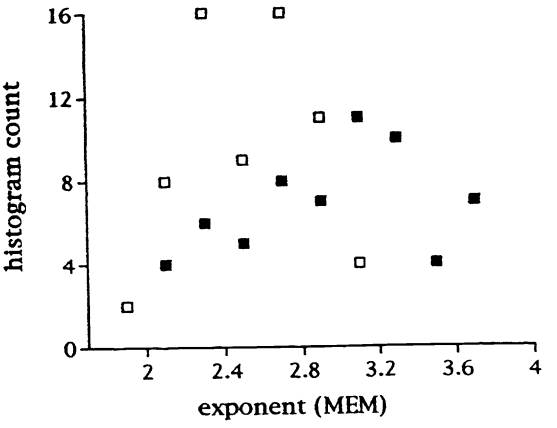

Figure 8. Histograms of power-law exponents for horizontal and vertical slices of the 65 mammogram records, measured using the MEM method.The open symbols are for a symbols are for a horizontal slice (f_x direction), solid symbols are for the vertical (f_y direction)

4.3. Sequential pixel variance analysis

One example of a spatial analysis of second-order statistics will be presented, based on a time-series analysis method adapted from Mandelbrot[29]. As will be discussed below, the result of this analysis is related to the estimated exponent of the power-law spectrum. The analysis was done as follows. A circle of diameter, D, was centered on each of the 65 square records previously used for spectral analysis. The mean and variance of the N_D pixel values, x_i, inside the circle were calculated. Pixel variance as a function of circle diameter, D, with mean, μ_D, is defined by

$$Var_D = \frac{1}{(N_D - 1)} \sum_{i=1}^{N_D} (x_i - \mu_D)^2 \text{ , for } N_D \text{ pixels in a circle of diameter D.} \quad (4)$$

The average variance and standard deviation of individual variances for the collection were determined.

This procedure was repeated for a range of circle diameters from 1.44 to 15.6 mm. The results are shown in figures 9 and 10. Note that logarithmic scales are used. The collection average variance increases as a power-law function of circle diameter. This is very different for the result that would have been obtained for uncorrelated white noise where the pixel variance would be constant, independent of circle diameter. The mean coefficient of variation [collection mean of individual image ROI standard deviation results]/collection mean of individual image ROI means results) is approximately constant for the collection of mammograms as circler diameter increases. The coefficient of variation for white noise decreases in proportion to $(N_D)^{-1/2}$, as expected.

The relationship between the sequential pixel variance and the power spectrum can be understand using the following argument, in 1D parameter space for convenience. The Wiener-Khinchine theorem[26] can be used to obtain a simple relationship between parameter variance, Var(x), the autocorrelation function, $R_{xx}(\tau)$ for shift, τ, and the volume under the 2D power spectrum, P(f). Given a zero-mean random process, x(t), with the continuous parameter, t, and frequency, f, the variance for an infinite measurement extent is

$$Var_\infty(x) = R_{xx}(0) = \int_{-\infty}^{\infty} P(f)df. \quad (5)$$

This relationship is only valid in the limit of infinite extent[30]. It is not possible to have continuous functions that have finite parameter support and are simultaneously band-limited. In the present context, one can regard infinity as a value much larger than the correlation distance of the noise in parameter space. Power-law noise does not have a unique correlation distance. For power spectra, $P(f) = 1/f^{\beta}$, the volume under the spectrum is infinite. This indicates that the variance, measured over infinite extent in the parameter space, will have an infinite value. The situation is very different for smoothed white noise filtered with defined correlation distance, ρ. Then the variance result will become constant when circle diameter is some relatively small multiple of ρ.

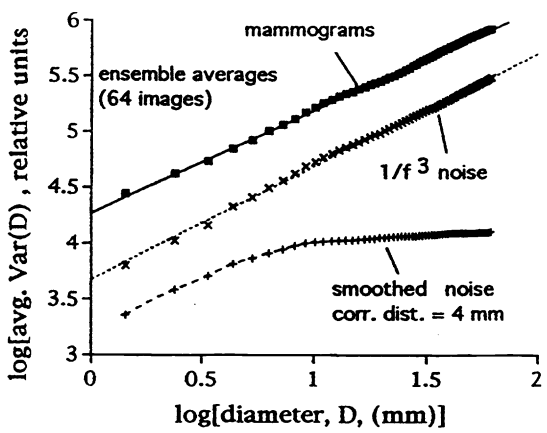

Figure 9 The mean value of sequential pixel variance measurements within circles of diameter , D, all with the same centers. The result is for 65 mammograms. The expected slope for a power-law process with spectrum $1/f^{\beta}$ is β-2. The measured slope for the mean result for 65 mammograms is 0.93. The $1/f^3$ noise (64 images) slope is 1.02. The smoothed noise result is constant for diameters much larger than the correlation distance.

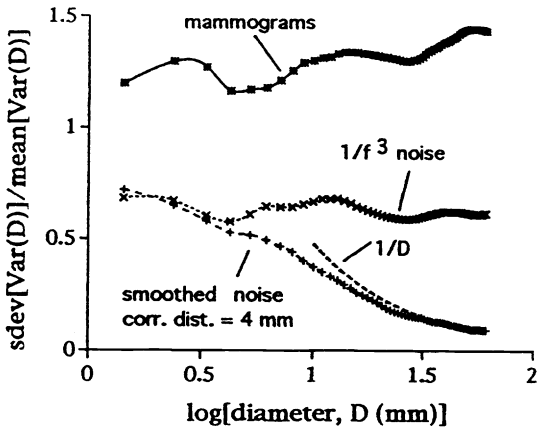

Figure 10. There is considerable variation in the sequential pixel variance results from image to image. This figure shows the measurement coefficient of variation (standard deviation/mean) for the 65 mammograms, $1/f^3$ noise, and for smoothed noise.

The 2D relationship between pixel variance and power spectrum volume for a finite circle area can be estimated by the following argument. Assume that the 2D power spectrum is isotropic with the form $P(f) = K/f^{\beta}$ where f is radial frequency. Assume that for the variance measurement, within a circle of diameter, D, the relationship between pixel variance and spectral density is given by the following polar integral, where the low frequency cut-off, f_0, equals D^{-1} (one cycle per circle diameter). Since the mean value is subtracted for each circle area, the DC component of the spectrum is not included in the calculation and f_0 is the lowest frequency included in the DFT estimate of spectrum for that circle diameter.

$$Var_D \approx 2\pi \int_{f_0}^{\infty} P(f) f df = 2\pi \int_{1/D}^{\infty} K f^{(1-\beta)} df = \frac{2\pi K}{(1-\beta)} \left[f^{(2-\beta)} \right]_{1/D}^{\infty} \text{ when } \beta > 2. \quad (6)$$

For values of the power-law exponent, β, greater than 2 and non-zero values of f_0 the result is

$$Var_D \approx K' f_0^{(2-\beta)} = K' D^{(\beta-2)}, \text{ with } K' = 2\pi K/(\beta-1). \quad (7)$$

Using the value of β equal 3 for the collection of 65 mammograms, one would expect the sequential pixel variance to be approximately proportional to measurement record diameter. This is exactly what was observed. Note that there is no evidence

for approach to a constant variance in figure 9. Pixel variance climbs steadily to the largest circle diameter. This suggests that the power spectrum is a power-law down to the lowest frequency evaluated. The relationship between collection average variance and circular record diameter appears to be consistent with power-law spectrum exponent estimates. The sequential pixel variance estimation procedure appears to be an attractive alternation that confines data analysis to the spatial domain.

5. TERMINOLOGY

5.1 General issues

Some authors use power-law slope and others use fractal-dimension to describe experimental results. Confusion can arise for two reasons. (1) Mathematicians, physicists and engineers frequently use different definitions and (2) authors often do not provide enough information to make it clear which definition is being used. One convenient reference for clarifying the problem is Voss[31]. The following is a summary of the issues.

5.2 Power-spectrum definition

There is an important distinction between defining an isotropic 2D power-spectral density function, P(f), as a slice of a 2D function, $P(f) = K/f^{\beta}$, (as is done in this paper) and defining a related function spectral density within an annulus of frequency range, Δf, using, $P^*(f)=K^*/f^{\beta^*}$, using with the * denoting an annulus-based function. The total spectral power is the same for the two cases but the integrands and Jacobians are different.

$$I = 2\pi \int_0^{\infty} P(f) f df = 2\pi K \int_0^{\infty} f^{(1-\beta)} df \quad \text{and} \quad I^* = \int_0^{\infty} P^*(f) df = K^* \int_0^{\infty} f^{-\beta^*} df = I \tag{8}$$

Multi-dimensional power-law processes have the interesting properties that both auto-correlation functions and power spectra are power-laws. In addition, slices and projections to lower dimensions also have related second-order statistics with power-law. This means that misinterpretations can occur very easily. So every word in a paper or book must be written and read with care to ensure that writer and reader are in step. Also it should be noted that, based on the projection-slice theorem[28], the power spectrum of fluctuations along any straight line on a fractal surface has a power spectrum $P_s(f) \approx 1/f^{\beta}$ with β in the range from 1 to 2.

5.3 Relationship between fractal-dimension and power-spectrum slope

From the definition of fractional Brownian motion, a fractal surface must have Hausdorf-Bescovich dimension, D (or sometimes D_H) fractal-dimension between 2 and 3. Let us assume the isotropic (no angular dependence) case. Using the slice definition for the radial 2D power-spectral density function and fractal-dimension, D as given by Voss[31] (page 70, equation 1.54) and Crilly et al.[32] (page 83) the relationships are given by

$$P(f_x, f_y) = \frac{K}{(f_x^2 + f_y^2)^{(4-D)}} \rightarrow P(f_r) = \frac{K}{f_r^{(8-2D)}} = \frac{K}{f_r^{\beta}} \quad \text{and} \quad \beta = 8 - 2D\,. \tag{9}$$

5.4 Definitions of β

It should be carefully noted that the slice-based spectral densities definitions used in this paper lead to a value of β that is *not* the same as that used by Voss[31] and many other authors. They use the exponent referred to as β^* in this manuscript, but they use the symbol β. Following the notation of 5.2, one obtains the annulus-spectral-density-based relationship

$$2D = 7 - \beta^*, \quad \text{or alternatively} \quad D = 2 + (3 - \beta^*)/2 \tag{10}$$

Equation (10), without the asterisk, has appeared in the medical physics literature several times without a clear indication as to whether the authors intended the slice or annulus definition of power- spectral density.

6. DISCUSSION

The preparation of an collection of normal CC mammograms has been described. Since the goal was to evaluate the statistical properties of breast tissue structure *per se*, it was necessary to eliminate the effects of organ thickness variation and the

nonlinear film response. Methods were developed to estimate the boundaries of the region where breast thickness was constant. The digitized image data were first converted to optical density scale and then to log-exposure scale using calibration data.

Spectral analysis was performed on 6.1 cm square region of an collection of 65 images. Both the DFT and MEM spectral estimates suggest a power-law spectrum, $N(f)=K/f^{\beta}$, with an average exponent value of about 3, with a range from 2 to 4. There appears to be a small variation of exponent with angle. The spectrum appears to become dominated by image noise for frequencies greater than 1 cycle/mm.

The sharp peak in the power spectrum presents a strong challenge to spectral analysis techniques. Both the DFT and MEM techniques are subject to systematic error. Fortunately, the errors tend to concentrate at opposite ends of the spatial frequency range. DFT results are suspect at low frequencies. The MEM results depend on the selected order of the Laurent series. If the order is too low then spectral estimates as all frequencies are affected. If the order is too high then systematic error appears to be concentrated at high frequency. Evaluation of MEM order selection using filtered noise appears to be useful.

The sequential pixel variance estimation procedure (performed in the spatial domain) appears to be an attractive alternative that confines data analysis to the spatial domain. Based on an approximation analysis, the power-law relationship between collection average variance and circular region diameter appears to be consistent with power-law spectrum exponent estimates. This method needs to be placed on a stronger mathematical footing.

This work should be regarded as a preliminary investigation of the statistical properties of mammographic breast tissue structure. Many questions remain to be answered. It is clear that methods must be developed to analyze smaller regions of interest so that statistical variation within individual breast images can be investigated. The detection of lesions in the presence of breast tissue structure is described in a separate paper[20].

ACKNOWLEDGEMENTS

I would like to thank a number of people. Larry Clarke, Maria Kallergi, John Heine and Robert Velthuizen of University of South Florida provided the digitized mammograms and a variety of related information. Jack Beutel and David Richards, Sterling Diagnostic Imaging, provided Min-R/Microvision H&D curve data. Phil Judy and Bijoy Misra of Brigham and Women's Hospital who were party to many discussions on all aspects of this work. Kyle Myers and Robert Wagner of CDRH took part in a number of helpful discussions. Ken Hanson, Los Alamos and Rodney Shaw, Hewlett-Packard Research Laboratories made helpful suggestions related to spectral analysis. This research was funded by grant R01-58302 from the US National Cancer Institute.

REFERENCES

[1] N. Petrick, H.P. Chan, B. Sahiner and D. Wei, "An adaptive density-weighted contrast enhancement filter for mammographic breast mass detection.," IEEE Trans. Med. Imag., **15**, 59-67 (1996)

[2] J.N. Wolfe, "Breast patterns as an index of risk of developing breast cancer," Am. J. Roentgenol. **126**, 1130-1139 (1976).

[3] J.W. Byng, N.F. Boyd, E. Fishell *et al.*, "The quantitative analysis of mammographic densities," Phys. Med. Biol. **39**, 1629-1638 (1994).

[4] C.E. Priebe, J.L. Solka, R.A. Lorey *et al.*, "The application of fractal analysis to mammographic tissue classification," Cancer Letters **77**, 183-189 (1994).

[5] P. Taylor, S. Hajnal, M.H. Dilhuydy *et al.*, "Measuring image texture to separate 'difficult'from 'easy' mammograms," Brit. J. Radiol. **67**, 456-463 (1994).

[6] J.W. Byng, N.F. Boyd, E. Fishell *et al.*, "Automated analysis of mammographic densities," Phys. Med. Biol. **41**, 909-923 (1996).

[7] B. Zheng, Y-H. Chang, and D. Gur, "Adaptive computer-aided diagnosis scheme of digitized mammograms," Acad. Radiol. **3**, 806-814 (1996).

[8] F.O. Bouchud, F.R. Verdun, J.F. Valley *et al.*, "The importance of anatomical noise in mammography," in *Medical Imaging 1997: Image Perception*, edited by H.L. Kundel (Proceedings of the Society of Photo-optical Instrumentation Engineers, Newport Beach, CA, 1997), Vol. 3036, pp. 74-80.

[9] C. Caldwell, S.J. Stapleton, D.W. Holdsworth *et al.*, "Characterisation of mammographic parenchymal pattern by fractal

dimension," Phys. Med. Biol. **35**, 235-247 (1990).
[10] J.W. Byng, N.F. Boyd, L. Little *et al.*, "Symmetry of projection in the quantitative analysis of mammographic images," European J. Cancer Prev. **5**, 319-327 (1996).
[11] S.M. Kay, *Modern Spectral Estimation, Theory and Application* (PTR Prentice Hall, Englewood Cliffs NJ, 1988).
[12] D.B. Percival and A.T. Walden, *Spectral Analysis for Physical Applications* (Cambridge University Press, Cambridge, 1993).
[13] J. Theiler, "Estimating fractal dimension," J. Opt. Soc. Am. **A7**, 1055-1073 (1990).
[14] Q Huang, JR Lorch, and RC Dubos, "Can the fractal dimension of images be measured?," Pattern Recognition **27**, 339-349 (1994).
[15] J.F. Veenland, J.L. Grashuis, F. van der Meer *et al.*, "Estimation of fractal dimension in radiographs," Med. Phys. **23**, 585-594 (1996).
[16] A.E. Burgess, "Bach, breasts and power law processes," to be submitted to Medical Physics.
[17] B. B. Mandelbrot, *The Fractal Geometry of Nature* (Freeman, New York, 1982).
[18] J.J. Heine, S.R. Deans, and L.P. Clarke, "Multiresolution probability analysis of random fields," J. Opt. Soc. Am. **A16**, 6-16 (1999).
[19] J.R. Rolland, "Higher order mammography statistics," presented at the OSA Annual Meeting, Baltimore, MD, 1998 (unpublished).
[20] A.E. Burgess, F.L. Jacobson, and P.F. Judy, "On the detection of lesions in mammographic structure," in *Medical Imaging 1999, Image Perception*, edited by E. Krupinski (Proceedings of the Society of Photo-optical Instrumentation Engineers, San Diego, CA, 1999), Vol. 3663, pp. to be published.
[21] M. Kallergi, M.A. Gavrieldes, W.W. Gross *et al.*, "Evaluation of a CCD-based film digitizer for digital mammography," in *Medical Imaging 1997: Physics of Medical Imaging*, edited by R.L. Van Metter and J. Beutel (Proceedings of the Society of Photo-optical Instrumentation Engineers, Newport Beach, CA, 1997), Vol. 3032, pp. 282-291.
[22] J. Beutel and D. Richards, private communication .
[23] IDL, Version 5.1 (Research Systems Inc., Boulder, CO, 1998).
[24] J.W. Byng, J.P. Critten, and M.J. Yaffe, "Thickness-equalization processing for mammographic images," Radiology **203**, 564-568 (1997).
[25] M.M. Goodsitt, H.P. Chan, B. Liu *et al.*, "Classification of compressed breast shapes for the design of equalization filters in x-ray mammography," Med. Phys. **25**, 937-948 (1998).
[26] J.S. Bendat and A.G. Piersol, *Random Data: analysis and measurement procedures* (John Wiley & Sons, New York, 1986).
[27] W.H. Press, B.P. Flannery, S.A. Teukolsky *et al.*, *Numerical Recipes in Fortran, Second Edition* (Cambridge Univ. Press, 1992).
[28] A. Papoulis, *Systems and Transforms with Applications in Optics* (MacGraw-Hill, New York, 1968).
[29] B.B. Mandelbrot, "New methods in statistical economics," J. Political Economy **71**, 421-440 (1963).
[30] D. Slepian, "Some comments on Fourier analysis, uncertainty and modelling," SIAM Review **25**, 1371-1430 (1983).
[1]R.F. Voss, "Fractals in nature: from characterization to simulation," in *The science of fractal images*, edited by M.F. Barnsley, R.L. Devaney, B.B. Mandlebrot *et al.* (Springer-Verlag, New York, 1988).
[32]A.J. Crilly, R.A. Earnshaw, and H. Jones, *Applications of Fractals and Chaos: The Shape of Things* (Springer-Verlag, New York, 1993).

Correspondence: e-mail: burgess@ulna.bwh.harvard.edu. Telephone: (617)732-6329; Fax: (617)732-6336